Domain Formation in Charged Polymer Vesicles

*Kaushik Chakraborty[1], Prabir Khatua[1], Wataru Shinoda[2], Sharon M. Loverde[1,3,4,5,]**

[1]Department of Chemistry, College of Staten Island, The City University of New York, 2800 Victory Boulevard, Staten Island, New York, 10314, United States

[2]Department of Materials Chemistry, Nagoya University, Furo-cho, Chikusa-ku, Nagoya 464-8603, Japan

[3]Ph.D. Program in Biochemistry, The Graduate Center of the City University of New York, New York, NY, 10016

[4]Ph.D. Program in Chemistry, The Graduate Center of the City University of New York, New York, NY, 10016

[5]Ph.D. Program in Physics, The Graduate Center of the City University of New York, New York, NY, 10016

E-mail: sharon.loverde@csi.cuny.edu, Phone: 718-982-4075,
Fax: 718-982-3910

Abstract

Microphase separation can occur on a polymersome membrane surface. The phase behavior depends on the mixture of charged and uncharged diblock copolymers and the salt concentration in solution. Using coarse-grained molecular dynamics simulations, we evaluate the elastic properties of mixed charged and uncharged diblock copolymer membranes as a function of charged polymer concentration for the case of divalent counterions in solution. We find that both the area elastic modulus and bending modulus increase with increasing charged copolymer concentration. We find that the membrane thickness decreases, and the membrane overlap increases with increasing charged copolymer concentration. We next perform large-scale simulations of a nearly 30 nm polymersome and characterize the growth of domains over 0.5 μs simulation time. We characterize the size, shape, and surface topology of the domains as they grow. These results add insight into the underlying mechanisms guiding the growth of domains in both synthetic and living cells.

INTRODUCTION

Biological surfaces are often highly inhomogeneous, with a wide range of components arranged in a quasi-regular pattern[1]. Nature has the unique ability to construct surfaces with specific patterns and topologies to perform various biological functions. For instance, nanometer and micrometer surface domains have been observed within cell membranes[2-4]. These domains are commonly known as 'rafts.' They are believed to play a crucial role, guiding various cellular processes, including budding, fusion, internalization, receptor transport, etc[3, 5, 6]. A similar kind of ordering with numerous functions is also observed within viral capsids and envelops[7].

Numerous experimental studies[8-10] have been performed on giant unilamellar vesicles to study raft dynamics. Rafts are usually achieved by mixing phospholipids with different chain lengths[11]. Analogous to natural phospholipid vesicles, polymer vesicles, commonly known as polymersomes[12, 13], are also model systems to mimic raft dynamics. Additionally, due to the wide range of building blocks, thickness, permeability, and mechanical properties of polymersomes are easily tunable compared to lipid vesicles. Furthermore, polymersomes can be designed to be pH, ionic environment, solvent, light, and temperature-sensitive. These attributes make polymersomes model stimuli-responsive soft materials as well as promising drug and gene delivery systems[14, 15]. Furthermore, these same attributes make polymersomes ideal biomimetic systems that can provide the underlying 'scaffolds' for the design of the synthetic cell or 'protocell'.[16, 17]

Fundamentally, using mixed polymer systems can allow for another dimension in controlling the materials properties, the shape, and the surface phase behavior of these model systems. For example, polymer-phospholipid blends have been shown to improve vesicle binding capabilities[18]. In order to engineer strong lateral phase segregation into mechanically robust polymersomes,

Discher et al. engineered[19, 20] vesicles composed by a mixture of anionic (poly (acrylic acid)-polybutadiene, PAA-PBD) and neutral (poly (ethylene oxide)-polybutadiene, PEO-PBD) di-block copolymers, that exhibit a fluid-gel transition in the presence of divalent cations. Divalent counterions condense and bridge the negatively charged PAA head groups, organizing the head groups into 'rafts.'[21] Moreover, *Bataglia et al.* [22]. demonstrated that polymer/polymer interactions can control the surface topology of polymersome domains. They created PEO domains with two surface topologies: elongated and circular or 2D micellar for a mixed spotted polymersome[23]. The surface topology of polymer vesicles also significantly impacts how these synthetically engineered systems interact with the living cell[24].

Membrane properties such as permeability and mechanical properties can be tuned based on the chemistry of the membrane components, ranging from polymer mixtures to incorporation of nanoparticles and synthetically designed or natural proteins[25]. Fundamentally, the thickness of polymer vesicle membranes can be tuned based on the molecular weight of the diblock copolymers[26]. At the same time, the area expansion modulus is set by the strength of the interfacial tension or the immiscibility of hydrophilic and hydrophobic blocks[26, 27]. The bending modulus, K_B, has been experimentally shown to scale with the thickness of the membrane such that $K_B \sim \beta K_A d^2$ where β is a prefactor that describes conformation and interdigitation of the upper and lower monolayers (degree of segregation) and d is the thickness of the bilayer[28]. At the molecular level, the contribution of intermolecular forces, particularly the electrostatic interactions, to the elastic properties of charged diblock copolymer membranes may depend on the local salt concentration, specifically the ratio of the Debye screening length with respect to the membrane width[29]. However, experimental results have shown that, for cationic vesicles composed of double-tailed cationic surfactant, the area elastic modulus is independent of the counterion concentration. In

contrast, the bending modulus displays a non-monotonic dependence[30]. It is predicted that a strongly absorbed counterion layer leads to a decrease in area expansion modulus and an increase in bending modulus[31, 32]. It is also shown that weakly charged membranes may increase bending rigidity, while highly charged membranes may possess a decreased bending rigidity[29]. Furthermore, it is predicted that the electrostatic contribution to the Gaussian modulus may destabilize charged membranes with respect to spherical deformation. As a function of surface charge, the bending rigidity of giant unilamellar vesicles (GUVs), characterized by shape fluctuation of the GUVs, increases [33]. However, the measured increase is lower than that predicted by theoretical models [34, 35].

Herein, using coarse-grained molecular dynamics simulations, we characterize the structural and elastic properties of mixed charged and uncharged diblock copolymer membranes. We use a mixture of polyacrylic acid (PAA)-polystyrene (PS) and polyethylene oxide (PEO)-PS as a model system. We find that the area expansion and bending modulus display differing trends concerning increasing surface charge than that shown for cationic surfactants,[30] due to the membrane properties and structure difference. Indeed, these results confirm that an increase in surface charge of a polymersome membrane *increases* the area expansion modulus, indicative of a fluid-gel transition, similar to that shown experimentally[27]. We also find that an increase in surface charge increases the bending rigidity.

Domains in synthetic and living cells have multiple contributions to their stability. Their phase behavior may be determined to some extent by the concentration of ions in the surrounding environment[19]. Indeed, ideal models show that the free energy of periodic microphases at low temperatures is the contribution of both the line tension and the electrostatic energy. In contrast,

at high temperatures, the free energy of mixing and counterion entropy have some contribution[36]. Here, we characterize the relative energy of larger domains and the time evolution of smaller domains in a mixture of charged and uncharged diblock copolymers confined to a membrane interface. We next perform large-scale coarse-grain simulations of a nearly 30 nm polymersome and characterize the growth of phase-segregated charged and uncharged domains over 0.5 μs simulation time. We attempt to accelerate domain growth using advanced sampling methods in molecular dynamics, considering multiple reaction coordinates to characterize the strength and coordination of polymer-polymer contacts. We find that larger pre-assembled domains have lower energy than smaller domains. This suggests that the lowest free energy state for these ionic conditions are larger, more strongly segregated domains. We next computationally characterize the relative contribution of counterion entropy, which is predicted to play a critical role in the microphase behavior of mixed ionic systems to the free-energy of multiple-sized domains. These results may add critical insight into the underlying molecular forces driving pattern formation in these model polymer membranes, as well as the living cell.

SIMULATION DETAILS

Continuum models can describe non-spherical topologies of fluid membranes and vesicles, as well as their dynamic evolution[37, 38]. Particle-based methods such as Monte Carlo (MC), Dissipative Particle Dynamics (DPD), and molecular dynamics (MD) can further characterize the shape transformation and stability of polymer vesicles, incorporating in-homogeneities within the membrane composition[39, 40]. In particular, coarse-grained molecular dynamics can give additional insight into the molecular driving forces guiding demixing or 'raft' formation in polymer or surfactant mixtures[20, 21]. Here, we report on coarse-grained molecular dynamics simulations of mixed charged and neutral diblock copolymers, both for a flat membrane morphology, as well as

a curved vesicle, or polymersome, morphology. We simulate a mixture of two different amphiphilic copolymers, both with hydrophilic fractions, $f_{EO,}$ that prefer the vesicle phase such that f_{EO} = 0.096. The number of EO (ethylene oxide) monomers, N_{EO}, plus the number of hydrophobic monomers, N_h, gives $N_{total} = N_{EO} + N_h$, and one can calculate $f_{EO}= N_{EO}m_{EO}/(N_{EO}\, m_{EO} + N_h m_h)$, where the m_i's are monomer masses that establish the total molecular weight of the polymer M_{tot}. Previously, we have shown that this PEO-polystyrene (PS) model with different copolymer lengths can also describe the characteristic partitioning of model hydrophobic solvents in the micellar phase[41]. The CG (coarse-grained) parameters for PEO were originally developed by *Shinoda et al.[42]. T*he CG parameters for PS are developed by our laboratory[43] using the Shinoda-DeVane-Klein (SDK) coarse-graining methodology. This approach has since been extended to the SPICA force field[44]. In the SDK methodology, intra-molecular interactions are given via bond and angle harmonic potentials fit to atomistic simulations as follows, $V_{\text{bond}}(r) = K_b(r - r_0)^2$ and $V_{\text{angle}}(\theta) = K_a(\theta - \theta_0)^2$. K_b is the equilibrium force constant and r_0 is the equilibrium bond radius. K_a is the equilibrium bending force constant and θ_0 is the equilibrium angle. Non-bonded interactions are given based on a slightly modified 9-16 or 12-4 pairwise additive potential based on the Lennard-Jones (LJ) potential: $U_{LJ9-6} = (27/4)\varepsilon\{(\sigma/r)^9 - (\sigma/r)^6\}$ or $U_{LJ12-4} = (3\sqrt{3}/2)\varepsilon\{(\sigma/r)^{12} - (\sigma/r)^4\}$ [45]. Next, to extend this model further, we include electrostatic interactions by incorporating a charged hydrophilic headgroup, mimicking the negatively charged polyacrylic acid (PAA) instead of PEO. We mimic the PAA by including a -1 charge on each CG (coarse grain) bead in the original PEO model. We mimic a model divalent Ca^{2+} counterion, with the radius on Na^{+1} from the original SDK force field[46] and including a +2 so that the overall system is electrically neutral. This model for Na^{+1} is parameterized based on capturing the surface tension for a range of Na Cl densities in water and assumes approximately two water molecules per coarse-

grained bead. The size of the Ca^{2+} bead could be adjusted to match structural properties such as the radial distribution function in atomistic simulations in further studies. All cross-interactions are described using a combination rule between *i* and *j*, where $\varepsilon_{ij} = \left(\varepsilon_{ii}\varepsilon_{jj}\right)^{1/2}$ and $\sigma_{ij} = (\sigma_{ii} + \sigma_{jj})/2$. While the polymersomes well-characterized by *Discher et al.* use mixed membranes composed by PAA-PBD and PEO-PBD, we utilize a mixture of PAA-PS and PEO-PS, since the force field for PS and PEO-PS diblock copolymers, as well as the elastic properties of their membrane assemblies, have been previously validated by our computational laboratory[47].

Four different polymer membranes with a varying fraction of charged PAA diblock copolymers (0%, 25 %, 50 %, and 75 %) are simulated in an aqueous medium. All bilayers contain 100 polymers with diblock lengths PEO_{11}-PS_{43} and PAA_{11}-PS_{43}, with 100,000 CG water molecules utilizing CG water parameters originally developed by *Shinoda et al.* [48]. Model Ca^{2+} ions are added to neutralize the system. The total number of beads in each system varies between 150000-200000. 0.5 μs trajectories are generated for each bilayer system with a time step of 10 fs. Simulations are performed under NPT conditions at 300 K and 1 atm using LAMMPS.[49] We use the Nose-Hoover thermostat[50] and Parrinello-Rahman barostat [51] and the equations of motion of Martyna et al. [52]. A summary of system sizes and configurations is given in **Table 1.**

Table 1. Summary of PEO_{11}-PS_{43} and PAA_{11}-PS_{43} mixed bilayer and polymersome systems.

System	$PAA_{11}PS_{43}$ Diblocks	$PEO_{11}PS_{43}$ Diblocks	Total CG beads	Total simulation time (μs)	Total CG water beads	Box Dimension Å^3	Total Ca^{2+} Ions

0:100	0	100	68,800	0.5	50,300	108x111x401	0
25:75	25	75	68,800	0.5	50,150	117x123x354	150
50:50	50	50	68,800	0.5	50,000	135x131x295	300
75:25	75	25	68,800	0.5	49,650	146x137x259	450
Polymersome (50:50) (E1)	650	650	659,400	0.5	415,000	372x353x363	3900
US1	650	650	659,400	0.25 (6x50 ns)	415,000	372x353x363	3900
US2	650	650	659,400	0.25 (6x50 ns)	415,000	372x353x363	3900
US3	650	650	659,400	0.25 (6x50 ns)	415,000	372x353x363	3900

Next, we set up a pre-assembled PAA-PS and PEO-PS mixed (50:50) polymersome structure with a diameter of around 30 nm. The inner core diameter is 150 Å, and the outer diameter is 250 Å, with a membrane thickness of ~ 50 Å that compares with the thickness of polymer membranes in the flat configuration with a thickness of 51 Å. The PAA-PS and PEO-PS diblocks are distributed randomly within the polymersome. Six different trials to find a representative stable polymersome

structure are performed. The number of polymers and the initial core radius of the polymersome is held constant while varying the number of polymers in the inner and outer leaflets. The water concentration in the center of the polymersome is also varied to find an equilibrium starting conformation. A schematic figure detailing the steps involved is shown in **SI 1.** First, we start with an equal number of polymers in the inner and outer leaflets of the polymersome of 650 polymers. As the initial system is not stable and exhibits significant membrane undulations, we next gradually move polymers from the inner leaflet to the outer leaflet keeping the total number fixed, 50 polymers at a time. Finally, the stable system contains 550 and 750 polymers in the inner and outer leaflets, respectively. Next, we vary the number of water molecules inside the polymersome to best approach an equilibrium structure of the polymersome. With a gradual increase in the number of waters inside, the polymersome adjusts water density inside by forming multiple pores in the membrane. This procedure is more thoroughly described in our previous publication[47]. We take the last stable configuration of the polymersome and continue the simulation for another 0.5 μs (E1). The mixed polymersome contains 650 PEO_{11}-PS_{43} diblock copolymers and 650 $PAA_{11}PS_{43}$ diblock copolymers. The polymersome system has 659,400 CG beads in total. This schematic procedure has also been described in detail in our previous publication (see Fig. 4 in main text and SI-1 and SI-3) in *Soft Matter*[47].

To test if we can further accelerate the formation of PAA and PEO microphase separated domain structures, we explore advanced sampling methods. We perform three umbrella sampling[53] (US1, US2, and US3) simulations with three different reaction coordinates using the COLVARS[54] module of LAMMPS. The self-coordination number (C_s) of the polymer head groups is considered as the reaction coordination for US simulations in order to accelerate domain growth.

C_s is defined as $C_s(group) = \sum_{i \in group} \sum_{j>i} \frac{1-(|x_i - x_j|/d_0)^n}{1-(|x_i - x_j|/d_0)^m}$, where d_0 is the cutoff distance, and n = 6 and m = 12 are the exponents. The sum is over all beads of a particular group, for example, PEO. Here d_0 is 6 Å. The value of d_0 is defined based on the radial distribution function, $g(r)$, of polymer head groups. Here C_s(PEO) and C_s(PAA) are the self-coordination numbers of PEO and PAA head groups respectively. C_s(PEO), C_s(PAA) and C_s(PEO)× C_s(PAA) are three different reaction coordinates that we consider. The third reaction coordinate is a product of the first two reaction coordinates. A harmonic potential (H) is applied for each US window, $H = \frac{1}{2}k(r_c - r_c^0)^2$, where k is the force constant with a value of 20 kcal mol^{-1}. r_c is the reaction coordinate, either C_s(PEO), C_s(PAA), or C_s(PEO)× C_s(PAA). For each US simulation, we run 6 windows with 50 ns each with a 2 ns equilibration in between each run. Finally, to obtain the potential of mean force (PMF) as a function of reaction coordinate, we use the weighted histogram analysis method (WHAM)[55, 56]. The centers for each US bin for US1 and US2 are 350, 450, 550, 650, 750, and 850. The centers for US3 are 350, 550, 1150, 1450, 1750, and 2050. Overlap between windows is shown in **SI 2.** All further results concerning umbrella sampling are shown in **SI 3**, **SI 4, SI 12** – **SI 17.**

Analysis

Stretching the Membrane. We artificially stretch each membrane along xy-plane by applying an external force with an umbrella sampling (US) simulation using the COLVARS module [54] in LAMMPS. $\frac{R_{xy}}{R_{xy}^0}$ is the reaction coordinate. Here $R_{xy} = R_x \times R_y$, R_x and R_y are the radius gyration of the membrane along the x and y direction, respectively and R_{xy}^0 is the value of R_{xy} for the tensionless state of the membrane. The radius of gyration is defined as $R_{x.y} =$

$\left(\frac{\sum_{i\in membrane}^{N}\left(r_{x,y}-r_{x,y,com}\right)^{2}}{N}\right)^{1/2}$. A harmonic potential (H) is applied for each US window with force constant k = 5 kcal mol^{-1}. For each membrane, we run 10 US windows with 50 ns each. Finally, to obtain the potential of mean force (PMF) as a function of the reaction coordinate, we use the weighted histogram analysis method (WHAM)[55, 56]. We next characterize the area elastic modulus, K_A, of the membranes. K_A is estimated from the slope of the tension (γ) vs. area expansion, ΔA/A. To do so, we stretch each membrane gradually along the xy-plane from its equilibrium structure (zero surface tension). After each stretching instance, we equilibrate the membrane for five ns, followed by a 50 ns production run. The final configuration of each production run is used as the starting configuration for the subsequent simulation of the membrane with increased area. We determine γ by using the formula, $\gamma = \langle (L_z/2)\,[(P_{zz} - (P_{xx} + P_{yy})/2)]\rangle$, where P_{ij} is the *ij* component of the pressure tensor and L_z is the box length along the z-axis. The calculation of γ along each of the trajectories has been carried out by averaging over five different blocks with ten ns duration. The error bar is calculated from the block averaging approach.

Bending Rigidity. We calculate the bending modulus (κ) of the membranes based on the polymer orientation fluctuation spectrum. Multiple methods exist to calculate the bending rigidity of membranes as a function of their thermal undulations, such as the height fluctuation method[57], and methods to analyze membrane response to applied forces[58]. However, here we choose the orientation fluctuation method to characterize the bending rigidities of these polymer membranes. This method has previously been developed and applied to phospholipid membranes and is suggested to be reliable down to shorter wavelengths[59, 60], but here we apply the same approach for polymer membranes. In short, κ is related to the fluctuations of polymer orientation [60, 61] such that $\langle |n^{||}{}_q|^2\rangle = \frac{K_B T}{q^2 \kappa}$. Here $n^{||}$ is the longitudinal component of the spectrum of the polymer

orientation. We define the polymer orientation by a vector connecting the two ends of the polymer hydrocarbon chain (PS chain) and several variations as discussed in the supporting information. To calculate κ for each membrane, we build a separate relatively large system with 2000 polymers and run for 110 ns.

Ion Entropy. The thermodynamic properties of the ions are calculated using the SPAM method[62]. Initially, the SPAM method (maps spelled in reverse) was applied to calculate the relative free energy difference between water molecules a the protein surface from the distribution of interaction energies between the water molecules and the environment[63]. Later, we also used this method to calculate the relative free energy of an encapsulated hydrophobic solvent in diblock copolymer micelles[41]. According to this method, the free energy of an ion can be represented as, $\boldsymbol{G_{SPAM} = -RT\, lnQ_{SPAM}}$, $\boldsymbol{Q_{SPAM}}$ is the partition function defined as $\boldsymbol{Q_{SPAM} = \sum_{E_S}[P(E_I)\, \exp(-\frac{E_I}{RT})]}$ where $P(\boldsymbol{E_I})$ is the probability of a ion having interaction energy $\boldsymbol{E_I}$ with its surroundings. Then, the entropic component ($\boldsymbol{S_S}$) can be calculated from $\boldsymbol{TS_S = < E_I > - G_{SPAM}}$ where $<\boldsymbol{E_I}>$ is the average energy of the ions. The interaction energy of the ions was calculated by computing the non-bonded energy of a tagged ion with its surroundings.

Results and Discussion

Membrane Structure

First, to characterize the effect of increasing charge membrane density on the membrane structure and elastic properties, we set up four different membranes, with an increasing fraction of charged polymers, Φ: 0%, 25%, 50%, and 75%. After 0.5 μs simulation time, the charged PAA starts to aggregate and form local domains as the divalent counterions condense on the polymer chains, bridging multiple PAAs together. For example, we show the final snapshot of the 50:50 membrane

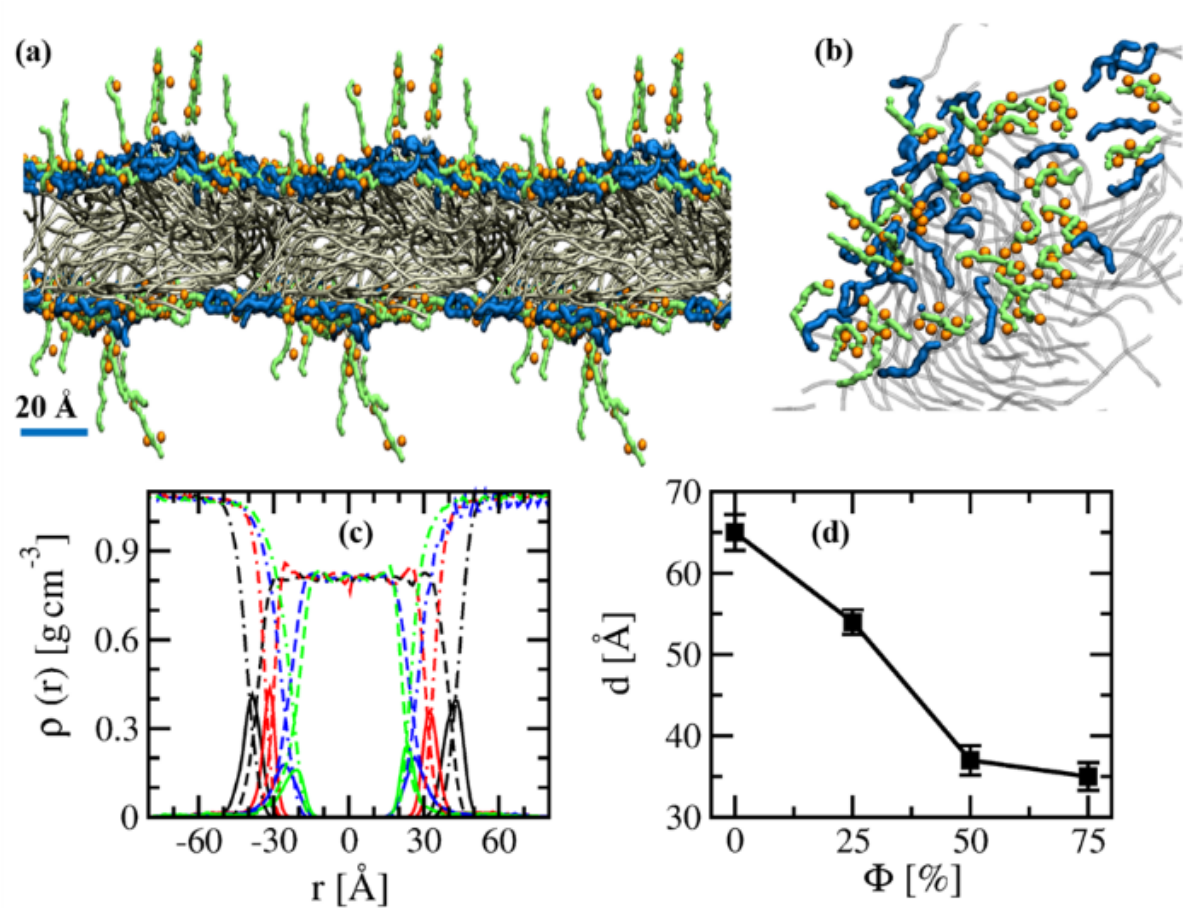

Figure 1. (a) Side view of a CG-MD (coarse grain molecular dynamics) simulation of a mixture of charged polyacrylic acid-polstyrene (PAA_{11}-PS_{43}) diblock copolymers and uncharged polyethylene oxide-polystyrene (PEO_{11}-PS_{43}) diblock copolymers in a membrane after 0.5 μs simulation. Here PS chains are shown in silver. PEO and PAA are in cyan and light green respectively. Ca^{2+} ions within 5 Å from the membrane are shown in orange. Water not shown. (b) Same system from a top view showing domain formation of charged PAA_{11}-PS_{43} diblock copolymers, with Ca^{2+} ions condensed on the PAA chains. (c) Density profiles, ρ(r) (g/cm^3), of PEO/PAA (solid line), PS (dotted line) and water (dot-dashed line) from the center of mass of the membrane. Black, red, blue, and green represent the data for four membranes with varying PAA fraction, Φ, 0%, 25%, 50%, and 75%. Variation of (d) width of the hydrophobic core, d, of the membrane with varying Φ.

after 0.5 μs simulation in **Figures 1 (a)** and **(b),** both from the side and tilted slightly from the top. Here PAA and PEO are in green and cyan, respectively. Ca^{2+} ions near the membrane surface are shown in orange.

Notably, with increasing the PAA fraction, the width of the hydrophobic core of the membrane decreases simultaneously (see **SI 5**). In addition, the PAA head groups stretch towards the water phase and interact strongly with the ions. An example of forming an ion-induced localized domain for the 50:50 membrane is shown in **Figure 1(b).** To further explore the membrane structure, we characterize the density profiles of both the head and tail groups of the diblock copolymers, as well as the water, in **Figure 1 (c)**. Compared to a neutral PEO-PS membrane, the head group density profiles of mixed PAA-PS and mixed PEO-PS membranes show a much broader distribution due to the PAA head groups' stretching towards the aqueous phase. The density profile of both charged (PAA) and neutral (PEO) heads groups separately is shown in **SI 6**. There is nearly 40 Å more extension of PAA towards the aqueous phase compared to PEO. The PAA is extended at the cost of decreasing entropy to gain enthalpic and electrostatic contacts with the counterions. Variation of the width of the hydrophobic core (d) of the bilayer is given in **Figure 1 (d)**. To compute d, first, we calculate the density fraction of PS (ρ_f) as a function of distance from the central core region. ρ_f is defined as $\frac{\rho_{PS}}{\rho_{PS}+\rho_{PEO}}$. Any regions with ρ_f greater than 0.9 are considered as a part of the membrane hydrophobic core. Hence, increasing the charge fraction of diblock copolymers makes the bilayer thinner. The width of the bilayer decreases from 65 Å to 35 Å by increasing the PAA fraction. There is also a corresponding increase in the surface area of the membrane with increasing the PAA fraction. **SI 7 (a)** shows the variation of the average surface area of each polymer, A_0. Repulsion between the PAA head groups results in an increased surface area of the membrane. To explore the effect of electrostatic repulsion between the head groups more

quantitatively, we compute the average interaction energy (E_H) of each of the polymer head groups with the rest of the polymer head groups present within the same leaflet and plot E_H) against A_0, as shown in **SI 7 (b)**. We observe a linear relationship between E_H and A_0. For a neutral membrane, PEO head groups experience a net van-der-Waals attractive force, but the incorporation of a negatively charge PAA head group increases the electrostatic repulsion and A_0 also increases simultaneously. Hence, the incorporation of charged head groups makes the mixed membrane thinner along the z-direction and longer along the xy-plane.

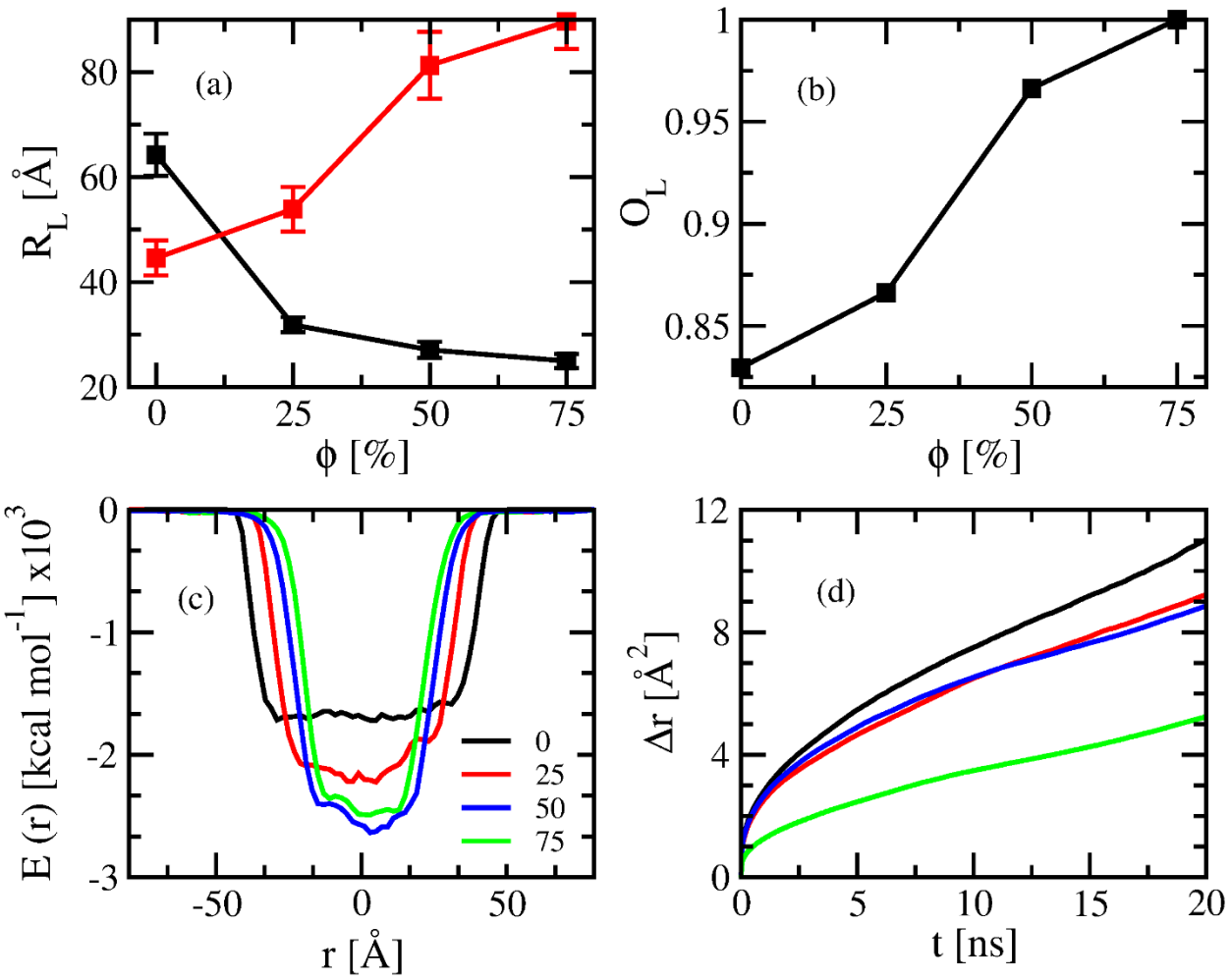

Figure 2. (a). End-to-end distance (R_L) of the hydrophobic PS chain along z-axis (black line) and xy-plane (red line) with varying PAA fraction, Φ, 0%, 25%, 50%, and 75% for membranes composed of mixed charged polyacrylic acid-polystyrene (PAA_{11}-PS_{43}) diblock copolymers and uncharged polyethylene oxide-polystyrene (PEO_{11}-PS_{43}) diblock copolymers. (b) Variation of overlap (O_L) between the two leaflets of the membrane with varying PAA fraction. (c) Variation of average cohesive energy density (E(r) (kcal/mol x 10^3)) across the membrane. (d) Mean-square-displacement (Δr^2 (Å^2)) of PS beads as a function of time in ns.

Such structural rearrangements may also alter the polymers' structure present within the bilayer's hydrophobic core. To characterize this, in **Figure 2 (a)**, we show the end-to-end distance (R_L) of the hydrophobic PS chain along the parallel (z-axis) and the perpendicular plane (xy-plane) of the membrane. Indeed, the presence of the charged head group impacts and stretches the PS chain along the perpendicular plane and reduces its length along the bilayer. This is consistent with the

increase in surface area and a decrease in the hydrophobic core width of the mixed membrane. Stretching of the PS chain along the xy-plane can also influence the extent of overlap between the two leaflets of the membrane. As shown in **Figure 2 (b)**, we characterize the fraction of overlap, or interpenetration of the two leaflets (O_P), with respect to total width, d, of the hydrophobic core, $O_P = \frac{d_p}{d}$. d_p is the overlapped region of the hydrophobic core, calculated from the density distributions of the upper and lower leaflets of the membrane. We define d_p as $(d_1 + d_2)/d$ where d_1 is the width of the top leaflet, d_2 is the width of the bottom leaflet, and d is the width of the hydrophobic core. The hydrophobic core thickness is defined as when hydrophobic density ρ_f is greater than or equal to 0.9. The same definition follows for d_1 and d_2. We find increased overlap from 0.83 to 1 with decreasing the width of the membrane due to the incorporation of the PAA head group. More overlap between the leaflets can also influence the energetics of the bilayer, especially for the hydrophobic core region. We compute the average cohesive energy density (E) across the membrane, as shown in **Figure 2 (c)**. Compared to the PEO-PS membrane, the cohesive energy of the hydrophobic core region is significantly higher for the mixed membrane. It increases gradually with increasing PAA fraction due to increased overlap between the upper and lower leaflets of the polymer bilayer. Besides energetics, the increased overlap between the membrane leaflets can also influence the mobility of the hydrophobic core. **Figure 2(d)** demonstrates the diffusion of the PS monomers as a function of time. The last 100 ns trajectory is used to calculate diffusion using a block averaging approach with five blocks of 20 ns each. We find lower diffusion by an order of magnitude of the PS chains for the mixed membranes compared to the pure PEO-PS membrane. In addition to the increased overlap between the membrane leaflets, the formation of a gel-like phase with the PAA and ions may lead to decreased diffusion.

Membrane Rigidity and Elasticity

In the previous section, we discuss the presence of charged polymer in the membrane and its consequent influence on the structure with increasing charge density. Increasing charge density is expected to modify the rigidity and elasticity of the membrane.

The potential of mean force (PMF) to laterally stretch the membrane calculated with umbrella sampling (US) is shown in **Figure 3 (a)**. The minima near $\frac{R_{xy}}{R_{xy}^{0}} = 1$ suggests that irrespective of the polymer bilayer, the lowest energy state is the tensionless state. The energy profiles further reveal that the free energy cost of stretching the membrane increases with increasing PAA fraction due to the hydrophobic core and the more gel-like character of the hydrophilic outer leaflet as it complexes with divalent counterions.

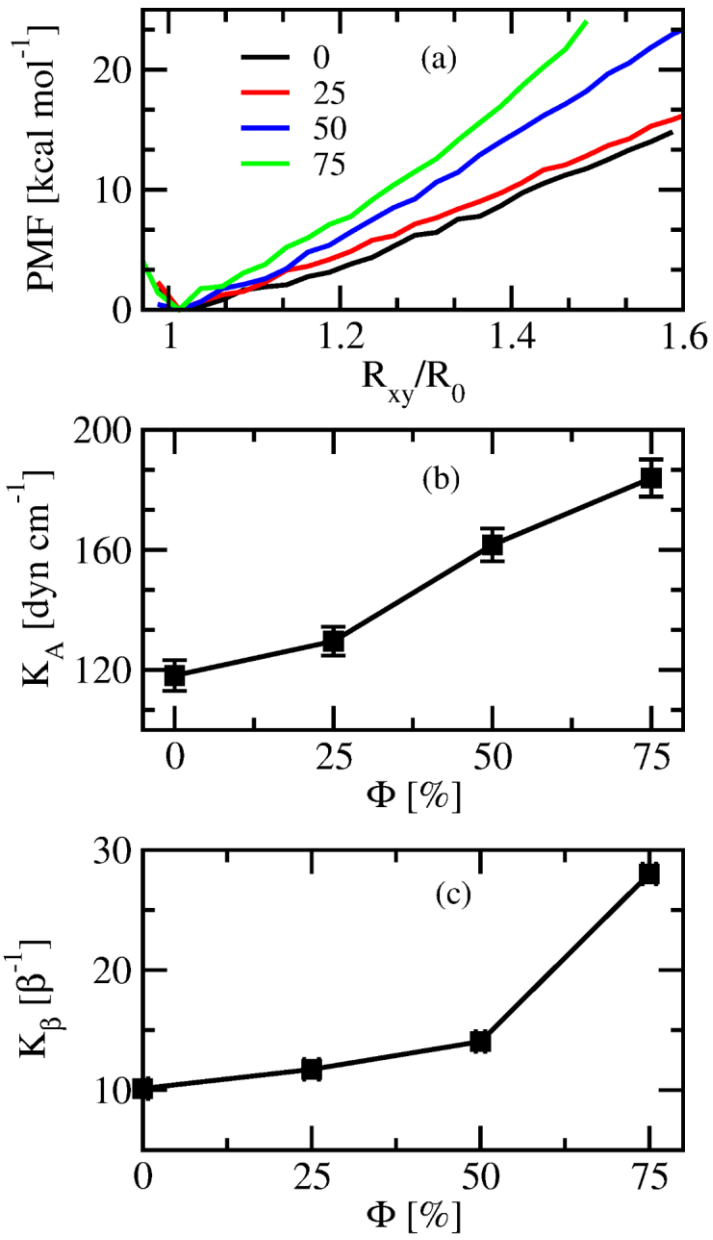

Figure 3. (a) Potential of mean force (PMF) (kcal/mol) of stretching the membranes along the xy-plane using $\frac{R_{xy}}{R_{xy}^0}$as the reaction coordinate. Variation of (b) the area elastic modulus, K_A (dyn/cm), and (c) the bending modulus (κ (1/β)) with varying PAA fraction.

We next characterize the area elastic modulus, K_A, by artificially stretching the membrane step by step, as given in the Analysis section. The variation of surface tension, γ, due to stretching for all

four membranes is shown in **SI 8.** Irrespective of the PAA fraction, artificially stretching the membrane shows an increase in surface tension**.** This has not been tested systematically experimentally, but this is easy to test in our simulation model. Variation of K_A with increased charged polymer fraction is shown in **Figure 3 (b)**. Consistent with the PMF, incorporating the charged head group also increases K_A by 40% for 75% PAA. These results also agree with experimental findings[19] that K_A increased by 20% with increasing pH from 4 to 6.

Furthermore, we next calculate the membranes' bending modulus (κ) based on the polymer orientation fluctuation spectrum. **SI 9** shows the variation of $n^{||}$, the longitudinal component of the spectrum of the polymer orientation, as a function of *q,* the wavenumber. Notably, in contrast to previous applications of the method to characterize the bending rigidities of phospholipid membranes[61], we find that this method is sensitive to the vector definition for each polymer orientation. This suggests that microscopic fluctuations are prominent at shorter wavelengths for these polymer membranes, as opposed to the phospholipid membranes this method has previously been applied to. Fitting the bending modulus to the selection of end-to-end vectors that shows the flattest slope, suggesting the least deviation from a continuum membrane, gives the variation of κ with increasing PAA fraction is shown in **Figure 3 (c)**. Like K_A, κ also increases gradually from 10.1 β^{-1} to 28.0 β^{-1} with increasing the PAA fraction. Hence, the presence of PAA head groups makes the bilayer relatively more rigid, and the results agree qualitatively with experimental findings by *Discher et al.* [19, 20].

Domain Formation

As shown in **Figure 1**, we see 'raft' or 'spot' formation due to localized segregation of the charged and neutral polymers. Cross-bridging between the negatively charged head groups of the polymer and divalent cations like Ca^{+2} and Cu^{+2} is mainly responsible for raft formation[19]. Instead of complete segregation of the charged and neutral polymers, we observe the formation of localized domains, leading to microphase separation. Our simulations thus also highlight the role of divalent ions in assisting the microphase separation. To investigate the role of ions in the microphase separation in detail, we first display the snapshots of the membranes as obtained at the end of 0.5 μs simulation in **Figures 4 (a)-(c)**, where we show Ca^{2+} ions within 5 Å from the membrane surface along with the PAA and PEO polymers. Many Ca^{2+} ions near the negatively charged PAA polymer

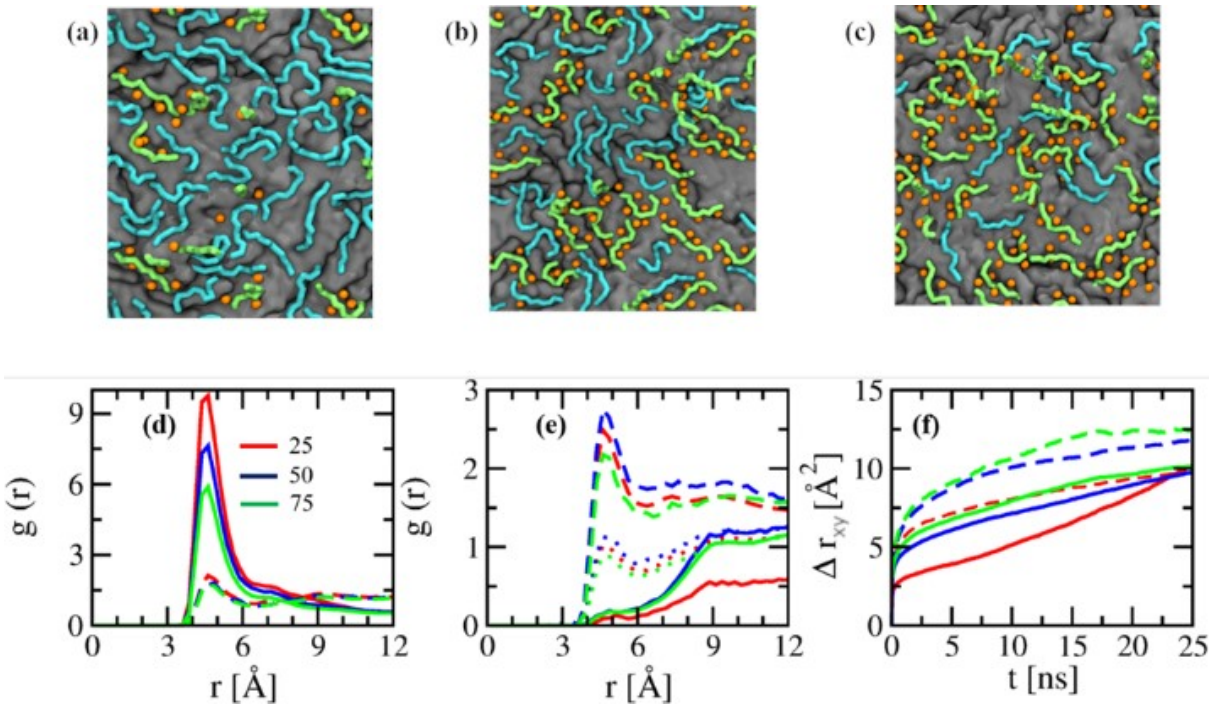

Figure 4. Snapshot of the membranes from the top after 0.5 μs simulation with (a) 25 %, (b) 50 %, and (c) 75 % PAA. PAA, PEO, PS, and Ca^{2+} ions are shown in green, cyan, gray, and orange respectively. (d) Pairwise correlation function $(g(r))$ of Ca^{2+} ions with respect to PAA (solid line) and PEO (dotted line) head groups. (e) $g(r)$ of PAA polymer head groups (solid line) , PEO (dashed line), and between PEO and PAA (dotted line). (f) Mean-square-displacements ($\Delta r_{xy}{}^2$) of PAA and PEO beads as a function of time in ns.

head groups condense on the PAA chains, bridging multiple headgroups into a domain. Indeed, almost 65% of the ions are condensed near the PAA head groups for the 50:50 mixed membrane. As shown in **Table 2**, the fraction of condensed Ca^{2+} ions varies with the charge fraction of the membrane.

Table 2. Summary of PEO_{11}-PS_{43} and PAA_{11}-PS_{43} mixed bilayer and polymersome systems.

System	Fraction (%) of condensed Ca^{2+} ions
25:75	43.41
50:50	64.59
75:25	63.79
Polymersome (E1)	85.46
Polymersome with domain (D1)	92.0

To probe the interactions between the polymer head groups and the Ca^{2+} ions further, we characterize the pairwise correlation function ($g(r)$) of the Ca^{2+} ions with respect to the PAA and PEO head groups of the diblock co-polymers as shown in **Figure 4 (d)**. A sharp peak around 4.5 Å suggests strong interactions of the PAA head groups with the Ca^{2+} ions. On the contrary, there is little interaction between the Ca^{2+} ions and the PEO head groups, as indicated by a lack of a peak. The $g(r)$ of polymer-polymer head groups is shown in **Figure 4 (e)**. The relatively large peak height indicates a more compact packing of PEO head groups compared to PAA. This correlates well with the net attraction and the strong electrostatic repulsion between the neutral and between the charged head groups of the polymers, respectively. The rate of segregation strongly depends on the lateral diffusion of the polymer. In **Figure 4 (f),** we show the mean-square-displacement of polymer head groups along the xy-plane $< \Delta r^2{}_{xy} >$ of the membrane. The lateral diffusion of PEO is relatively faster than the PAA. This may be due to the strong interactions of Ca^{2+} ions with the PAA.

Domain Formation in Mixed Polymersomes.

We have discussed so far how the presence of divalent ions drives the formation of localized domains in a membrane made of charged and neutral polymers that leads to microphase separation. Now, we scrutinize the thermodynamic driving force and plausible pathway of forming such a localized domain in a polymersome. For this, we prepare a pre-assembled polymersome consist of 50:50 charged PAA and neutral PEO polymers following the procedure as described in the **Methods** section. At first, we visualize the simulated trajectories and find localized segregation of both the charged (PAA) and neutral (PEO) head groups (see **Figures 5(a)** and **SI 11**). Formation of such a localized domain both from the charged and neutral polymer is further confirmed in **Figure 5 (b),** where we show the time evolution of the number of domains (D_N). Here, we consider a domain formed by a specific type of polymer monomers (charged or neutral) if the two monomers are within ≤ 4 Å. In the beginning, the high value of D_N for both PAA and PEO suggests that the PAA and PEO are spread homogeneously on the polymersome membrane surface without any localized segregation. However, a sharp decrease in D_N within a very short time (~10 ns) clearly illustrates the formation of a larger domain, which is particularly true for neutral PEO polymer. On the other hand, while we also observe the decrease in D_N with respect to the initial value for charged polymer, the change is much lower than PEO polymer. This suggests that the likeliness of domain formation by the PAA polymer is lower than the neutral polymer due to electrostatic repulsion between these charged polymers. To examine the domains further, we compute the size of the domain (D_S), the number of polymers in a domain. The comparison of domain size distribution suggests that PEO polymers form a relatively larger domain than PAA polymers (**Figure 5 (c)**), as evident from the spread of the distribution towards a relatively higher value for PEO polymers. However, interestingly, we see no noticeable difference between the size of the

most populated domain for either of the polymers. Therefore, it raises the question — whether are the larger domains at all thermodynamically stable? To address this question, we compute the cohesive energy (E) of PAA and PEO head groups under two circumstances (i) as a part of a domain with at least five polymers, representative of the sufficiently large domain (ii) as a unimer. The distribution of the cohesive energy under these two circumstances is shown in **Figure 5 (d).** Irrespective of the nature of the polymer, the formation of larger domains is thermodynamically favorable as clear from the relatively more negative value of E for the larger domain than when there is no domain. Besides, we see that domains formed by PAA are even more thermodynamically favorable than those formed by neutral PEO polymer. This further raises two questions: (i) why are PAA domains formed despite having strong electrostatic repulsion between them? (ii) why do PEO polymers tend to form a relatively larger domain than the PAA domain despite being relatively less thermodynamically favorable (see **Figure 5 (c)**)? The first question can be answered in line with what we observed in the case of the mixed membrane as discussed in the previous section, which illustrates that the divalent cations condense near the negatively charged PAA polymers (see **Figures 4 (a)-(c)** and **Figure 5 (a)**) and thereby help bridge these polymers by minimizing the electrostatic repulsion between them. The rate of segregation of these domains depends on the diffusion of the PEO and the PAA. PAA polymers move more slowly due to the strong electrostatic attraction between the PAA polymers and divalent cations. This slows down the rate of PAA domain formation and rearrangement. In other words, PAA domains are kinetically trapped in a gel-like configuration, but as shown by the cohesive energy, they provide a more negative contribution to the enthalpic energy. Thus, we notice a sharp decrease in the number of domains for PEO on a relatively faster time scale than that for PAA domains (see **Figure 5 (b)**) due to the faster PEO diffusion.

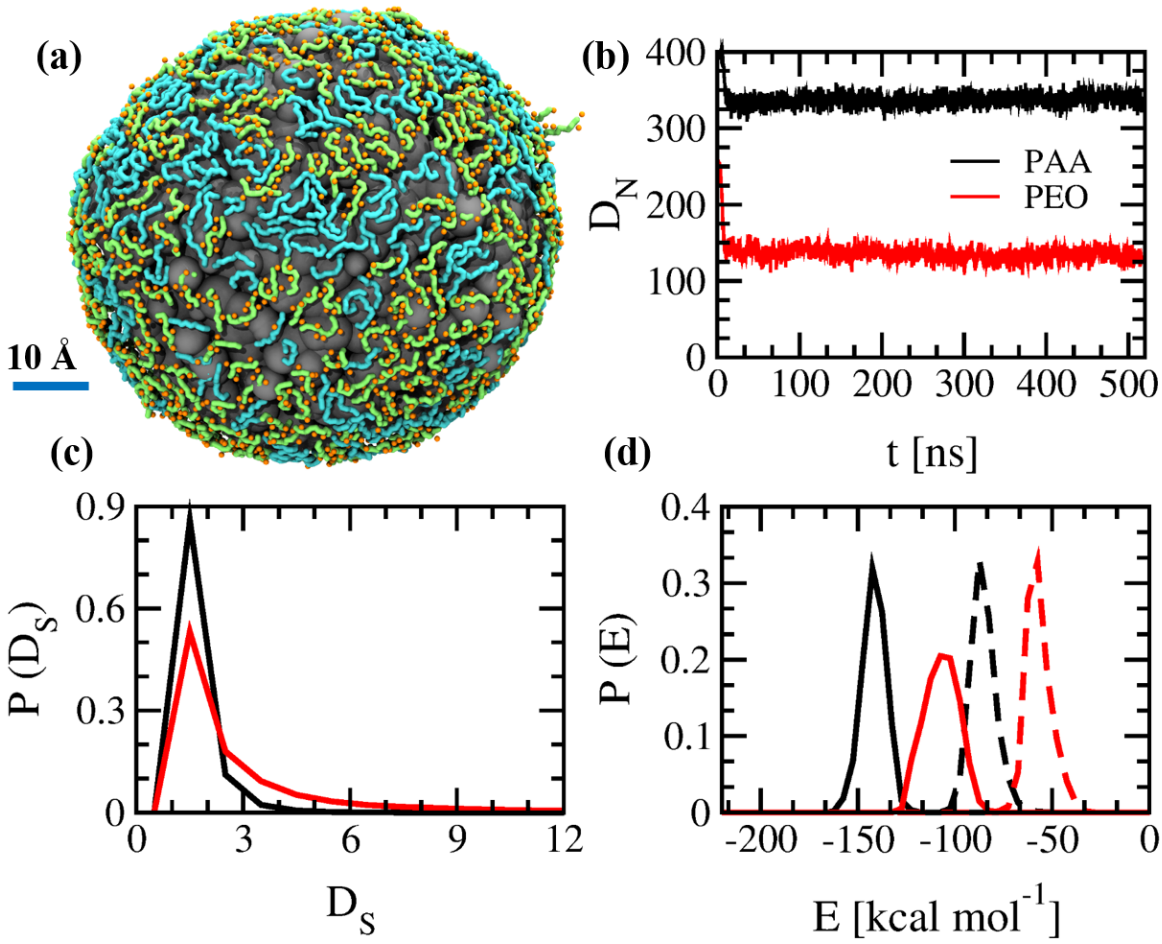

Figure 5. (a) Final snapshot of mixed polymersome composed 650 $PEO_{11}PS_{43}$ diblock copolymers and 650 $PAA_{11}PS_{43}$ diblock copolymers after 0.5 μs equilibrium simulation (E1). PEO, PAA, and PS are shown in cyan, green, and gray respectively. Ca^{2+} ions are in orange. (b) Variation of PEO and PAA domain numbers (D_N) as a function of time. (c) Distributions of PEO and PAA domain size (D_S) over the last 400 ns simulation. (d) Cohesive energy (E (kcal/mol)) distributions of PEO and PAA. Solid lines represent the data when the head group is a part of a domain with at least five polymers and dotted lines when the head group is a part of a domain with one polymer only.

The formation of localized PAA domains should possess a relatively higher energy barrier than that for PEO domains due to the slower diffusion of PAA polymers. However, PAA domains are energetically more favorable than the ones for neutral PEO polymers. Moreover, it has also been shown that both domains are thermodynamically favorable. To test this hypothesis, we take the final configuration of the E1 simulation and artificially place similar kinds of polymers next to each other to increase the overall size of each of the two types of domains. This artificially prepared pre-assembled mixed polymersome system is simulated for 60 ns duration. We find that artificially created domains expectedly remain stable throughout the simulation. Here, we show only the final snapshot as obtained at the end of the D1 simulation in **Figure 6 (a)**. The total energy (E_T) of this artificially created polymersome is an order of magnitude lower than the one from the E1 system (**Figure 6 (b)**). To scrutinize the energetics of domains more closely, we calculate the cohesive energy (E) separately for the head and tail groups of each of the two types of domains in such an artificially prepared system. We compare the data with that obtained from the E1 system. The distributions of the cohesive energy for the head and tail groups are depicted in **Figures 6 (c)** and **(d)**, respectively. PAA domains are energetically more stable than PEO domains, irrespective of whether the calculation is done for the head or tail group. While both PAA and PEO have similar energetic distributions for the PS tails, the energy distribution for the PAA head groups has more negative values than that for PEO. This confirms that the PAA domains are indeed inherently more stable than PEO domains. A closer inspection of the data further reveals that domains become even more stable on increasing the domain size with the effect being more for charged polymer irrespective of the polymer types. This once again confirms that PAA domains are more stable than PEO domains, but their formation is kinetically slower due to the slower diffusion of charged

PAA polymers. Thus, domain formation is an enthalpically favorable process but diffusion controlled.

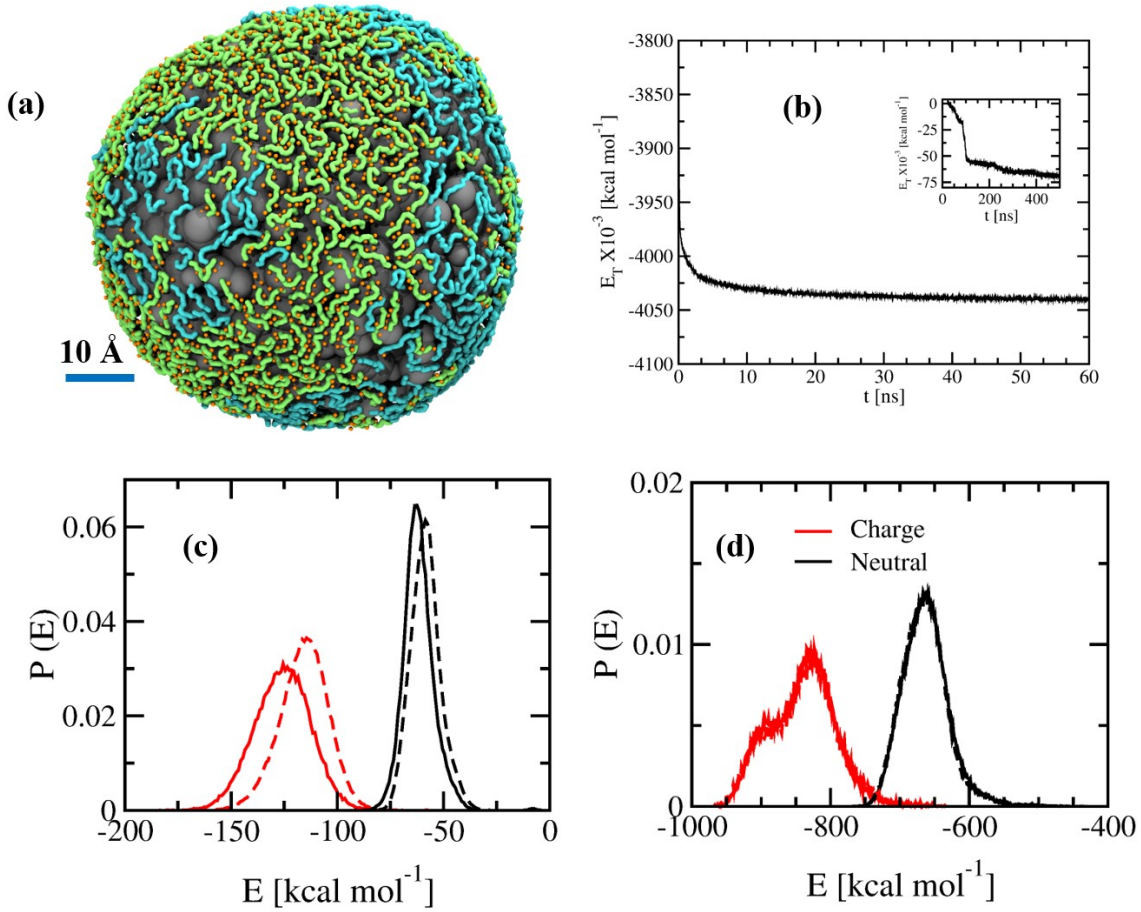

Figure 6. (a) Final snapshot of mixed $PEO_{11}PS_{43}$ and $PAA_{11}PS_{43}$ polymersome with a pre-assembled larger domain (D1) after 60 ns. (b) Variation of total energy (E_T (kcal/mol x 10^3) of D1 simulation. Variation of E_T for E1 simulation is also incorporated in the inset. Distributions of energy (E (kcal/mol)) of (c) head and (d) tails groups of the PAA-PS and PEO-PS polymers. Solid and dotted lines represent the data for D1 and E1 simulation respectively.

The Ca^{2+} ions play a critical role in stabilizing the charged domains. To explore the role of these ions in more detail, we compute their thermodynamic properties using the SPAM method as defined in the analysis section. We specifically investigate the thermodynamic properties of ions under two very different environments: *i)* first when they are interacting with neighboring charged

PAA, forming larger domains (at least with five polymers, D_S (5)) and, *ii)* secondly, when they are interacting with neighboring PAA forming a singular domain (one polymer only, D_s (1)). The corresponding *P* (E_I) distributions are shown in **SI 12.** Surprisingly, the distribution for D_S (5) suggests higher entropy than D_S (1). Detailed values of the thermodynamic properties are given in **Table 3**. Thus, these results suggest that Ca^{2+} ions interacting with PAA are free energetically more stable due to their comparably larger entropy. The ions within a large 'raft' can pass from chain to chain and thus explore a larger configurational space than those bound to an isolated chain.

Table 3. Thermodynamic properties of ions as a part of big domain (D_S(5)) and as a part of small domain with only one polymer (D_S(1)). Data for both umbrella sampling simulations and D1 simulations are shown in the table.

Properties	D_s (5) [kcal mol^{-1}]		D_s (1) [kcal mol^{-1}]		Δ [kcal mol^{-1}]	
	Umbrella sampling simulations	E1 simulation	Umbrella sampling simulations	E1 simulation	Umbrella sampling simulations	E1 simulation
G	-275.09 (±3.50)	-249.06 (± 3.99)	-214.07 (±2.89)	-213.01 (±2.93)	-51.02	-36.05
H	-180.42 (±4.92)	-163.59 (± 5.01)	-167.75 (±3.02)	-166.01 (± 3.10)	-51.02	2.42
TS	94.67 (±3.10)	86.47(± 3.25)	46.317 (±2.65)	47.00 (± 2.60)	48.32	39.47

Conclusion

Herein, we study the structural and mechanical properties of mixed polymer bilayers with varying charge fraction. These results suggest that a bilayer membrane becomes thinner and flatter by

incorporating a charged amphiphile, PAA-PS. As a result, the overlap between the hydrophobic cores of the two leaflets increases significantly. In addition, the counterions in the surrounding medium condense and bridge the charged amphiphiles, forming localized domains. Moreover, we find that these gel-like membranes are harder to stretch and bend, as indicated by their higher area elastic modulus and bending modulus. These results are consistent with previous experimental observations[19, 20]. By screening the charge interactions, divalent ions stabilize the charged domains while the ions gain entropy. In agreement with recent experimental studies[23], we also observe differing shapes for charged and neutral domains. We find neutral domains form 2D micellar topologies as well as elongated domains. In contrast, charged domains tend to elongate and stretch.

Next, we explore the domain formation pathways in a nearly 30 nm diameter mixed polymersome using advanced sampling methods. Preliminary results indicate that a careful choice of reaction coordinate is necessary, and further investigations need to be performed. Besides these synthetic polymersomes, these same underlying molecular mechanisms may drive the formation of biological domains in complex cell membranes.

ASSOCIATED CONTENT

Supporting Information. Figures S1-S17 contain a schematic sketch of polymersome equilibration, further details on the structure and mechanical properties of membranes, additional snapshots, free energy, and shape of domains for umbrella sampling calculations

AUTHOR INFORMATION

Corresponding Author

sharon.loverde@csi.cuny.edu

Author Contributions

The manuscript was written through the contributions of all authors. All authors have approved the final version of the manuscript.

Funding Sources. NSF Grant DMR-1750694

Acknowledgments. S. M. L. acknowledges start-up funding received from College of Staten Island and City University of New York. S. M. L. would also like to acknowledge NSF Grant DMR-1750694.

REFERENCES

1. Chaffey, N. Alberts, B., Johnson, A., Lewis, J., Raff, M., Roberts, K. And Walter, P. Molecular Biology of the Cell. 4th Edn. *Ann Bot* **2003,** 91 (3), 401-401 DOI: 10.1093/aob/mcg023.
2. Eggeling, C.; Ringemann, C.; Medda, R.; Schwarzmann, G.; Sandhoff, K.; Polyakova, S.; Belov, V. N.; Hein, B.; von Middendorff, C.; Schönle, A.; Hell, S. W. Direct Observation of the Nanoscale Dynamics of Membrane Lipids in a Living Cell. *Nature* **2008,** 457, 1159 DOI: 10.1038/nature07596

https://www.nature.com/articles/nature07596#supplementary-information.
3. Simons, K.; Ikonen, E. Functional Rafts in Cell Membranes. *Nature* **1997,** 387 (6633), 569-572 DOI: 10.1038/42408.
4. Gaus, K.; Gratton, E.; Kable, E. P. W.; Jones, A. S.; Gelissen, I.; Kritharides, L.; Jessup, W. Visualizing Lipid Structure and Raft Domains in Living Cells with Two-Photon Microscopy. *Proceedings of the National Academy of Sciences* **2003,** 100 (26), 15554 DOI: 10.1073/pnas.2534386100.
5. Jacobson, K.; Mouritsen, O. G.; Anderson, R. G. W. Lipid Rafts: At a Crossroad between Cell Biology and Physics. *Nature Cell Biology* **2007,** 9, 7 DOI: 10.1038/ncb0107-7.
6. Anderson, R. G. W.; Jacobson, K. A Role for Lipid Shells in Targeting Proteins to Caveolae, Rafts, and Other Lipid Domains. *Science* **2002,** 296 (5574), 1821 DOI: 10.1126/science.1068886.
7. Grünewald, K.; Desai, P.; Winkler, D. C.; Heymann, J. B.; Belnap, D. M.; Baumeister, W.; Steven, A. C. Three-Dimensional Structure of Herpes Simplex Virus from Cryo-Electron Tomography. *Science* **2003,** 302 (5649), 1396 DOI: 10.1126/science.1090284.
8. Baumgart, T.; Hess, S. T.; Webb, W. W. Imaging Coexisting Fluid Domains in Biomembrane Models Coupling Curvature and Line Tension. *Nature* **2003,** 425 (6960), 821-824 DOI: 10.1038/nature02013.
9. Yanagisawa, M.; Imai, M.; Taniguchi, T. Shape Deformation of Ternary Vesicles Coupled with Phase Separation. *Physical Review Letters* **2008,** 100 (14), 148102 DOI: 10.1103/PhysRevLett.100.148102.
10. Korlach, J.; Schwille, P.; Webb, W. W.; Feigenson, G. W. Characterization of Lipid Bilayer Phases by Confocal Microscopy and Fluorescence Correlation Spectroscopy. *Proceedings of the National Academy of Sciences* **1999,** 96 (15), 8461 DOI: 10.1073/pnas.96.15.8461.

11. Veatch, S. L.; Keller, S. L. Separation of Liquid Phases in Giant Vesicles of Ternary Mixtures of Phospholipids and Cholesterol. *Biophys J* **2003,** 85 (5), 3074-3083 DOI: 10.1016/S0006-3495(03)74726-2.
12. Discher, B. M.; Won, Y.-Y.; Ege, D. S.; Lee, J. C. M.; Bates, F. S.; Discher, D. E.; Hammer, D. A. Polymersomes: Tough Vesicles Made from Diblock Copolymers. *Science* **1999,** 284 (5417), 1143 DOI: 10.1126/science.284.5417.1143.
13. Discher, D. E.; Eisenberg, A. Polymer Vesicles. *Science* **2002,** 297 (5583), 967 DOI: 10.1126/science.1074972.
14. Lomas, H.; Canton, I.; MacNeil, S.; Du, J.; Armes, S. P.; Ryan, A. J.; Lewis, A. L.; Battaglia, G. Biomimetic Ph Sensitive Polymersomes for Efficient DNA Encapsulation and Delivery. *Advanced Materials* **2007,** 19 (23), 4238-4243 DOI: 10.1002/adma.200700941.
15. Ahmed, F.; Pakunlu, R. I.; Brannan, A.; Bates, F.; Minko, T.; Discher, D. E. Biodegradable Polymersomes Loaded with Both Paclitaxel and Doxorubicin Permeate and Shrink Tumors, Inducing Apoptosis in Proportion to Accumulated Drug. *Journal of Controlled Release* **2006,** 116 (2), 150-158 DOI: https://doi.org/10.1016/j.jconrel.2006.07.012.
16. Kamat, N. P.; Katz, J. S.; Hammer, D. A. Engineering Polymersome Protocells. *Journal of Physical Chemistry Letters* **2011,** 2 (13), 1612-1623 DOI: 10.1021/jz200640x.
17. Mason, A. F.; Thordarson, P. Polymersomes as Protocellular Constructs. *Journal of Polymer Science Part a-Polymer Chemistry* **2017,** 55 (23), 3817-3825 DOI: 10.1002/pola.28780.
18. Cheng, Z. L.; Elias, D. R.; Kamat, N. P.; Johnston, E. D.; Poloukhtine, A.; Popik, V.; Hammer, D. A.; Tsourkas, A. Improved Tumor Targeting of Polymer-Based Nanovesicles Using Polymer-Lipid Blends. *Bioconjugate Chemistry* **2011,** 22 (10), 2021-2029 DOI: 10.1021/bc200214g.
19. Christian, D. A.; Tian, A.; Ellenbroek, W. G.; Levental, I.; Rajagopal, K.; Janmey, P. A.; Liu, A. J.; Baumgart, T.; Discher, D. E. Spotted Vesicles, Striped Micelles and Janus Assemblies Induced by Ligand Binding. *Nature Materials* **2009,** 8, 843 DOI: 10.1038/nmat2512

https://www.nature.com/articles/nmat2512#supplementary-information.
20. Spinler, K.; Tian, A.; Christian, D. A.; Pantano, D. A.; Baumgart, T.; Discher, D. E. Dynamic Domains in Polymersomes: Mixtures of Polyanionic and Neutral Diblocks Respond More Rapidly to Changes in Calcium Than to Ph. *Langmuir* **2013,** 29 (24), 7499-7508 DOI: 10.1021/la304602e.
21. Pantano, D. A.; Moore, P. B.; Klein, M. L.; Discher, D. E. Raft Registration across Bilayers in a Molecularly Detailed Model. *Soft Matter* **2011,** 7 (18), 8182-8191 DOI: 10.1039/c1sm05490b.
22. LoPresti, C.; Massignani, M.; Fernyhough, C.; Blanazs, A.; Ryan, A. J.; Madsen, J.; Warren, N. J.; Armes, S. P.; Lewis, A. L.; Chirasatitsin, S.; Engler, A. J.; Battaglia, G. Controlling Polymersome Surface Topology at the Nanoscale by Membrane Confined Polymer/Polymer Phase Separation. *ACS Nano* **2011,** 5 (3), 1775-1784 DOI: 10.1021/nn102455z.
23. Ruiz-Pérez, L.; Messager, L.; Gaitzsch, J.; Joseph, A.; Sutto, L.; Gervasio, F. L.; Battaglia, G. Molecular Engineering of Polymersome Surface Topology. *Science Advances* **2016,** 2 (4), e1500948 DOI: 10.1126/sciadv.1500948.
24. Massignani, M.; LoPresti, C.; Blanazs, A.; Madsen, J.; Armes, S. P.; Lewis, A. L.; Battaglia, G. Controlling Cellular Uptake by Surface Chemistry, Size, and Surface Topology at the Nanoscale. *Small* **2009,** 5 (21), 2424-2432 DOI: 10.1002/smll.200900578.
25. Le Meins, J. F.; Sandre, O.; Lecommandoux, S. Recent Trends in the Tuning of Polymersomes' Membrane Properties. *European Physical Journal E* **2011,** 34 (2), DOI: 10.1140/epje/i2011-11014-y.
26. Bermudez, H.; Brannan, A. K.; Hammer, D. A.; Bates, F. S.; Discher, D. E. Molecular Weight Dependence of Polymersome Membrane Structure, Elasticity, and Stability. *Macromolecules* **2002,** 35 (21), 8203-8208.

27. Christian, D. A.; Tian, A.; Ellenbroek, W. G.; Levental, I.; Rajagopal, K.; Janmey, P. A.; Liu, A. J.; Baumgart, T.; Discher, D. E. Spotted Vesicles, Striped Micelles and Janus Assemblies Induced by Ligand Binding. *Nature materials* **2009,** 8 (10), 843-9.
28. Bermudez, H.; Hammer, D. A.; Discher, D. E. Effect of Bilayer Thickness on Membrane Bending Rigidity. *Langmuir* **2004,** 20 (3), 540-543 DOI: 10.1021/la035497f.
29. Nguyen, T. T.; Rouzina, I.; Shklovskii, B. I. Negative Electrostatic Contribution to the Bending Rigidity of Charged Membranes and Polyelectrolytes Screened by Multivalent Counterions. *Physical Review E* **1999,** 60 (6), 7032-7039 DOI: 10.1103/PhysRevE.60.7032.
30. Seth, M.; Ramachandran, A.; Leal, L. G. Direct Measurements of Effect of Counterion Concentration on Mechanical Properties of Cationic Vesicles. *Langmuir* **2013,** 29 (46), 14057-14065 DOI: 10.1021/la403329h.
31. May, S. Curvature Elasticity and Thermodynamic Stability of Electrically Charged Membranes. *Journal of Chemical Physics* **1996,** 105 (18), 8314-8323 DOI: 10.1063/1.472686.
32. Shoemaker, S. D.; Vanderlick, T. K. Intramembrane Electrostatic Interactions Destabilize Lipid Vesicles. *Biophys J* **2002,** 83 (4), 2007-2014.
33. Faizi, H. A.; Frey, S. L.; Steinkuhler, J.; Dimova, R.; Vlahovska, P. M. Bending Rigidity of Charged Lipid Bilayer Membranes. *Soft Matter* **2019,** 15 (29), 6006-6013 DOI: 10.1039/c9sm00772e.
34. Lekkerkerker, H. N. W. Contribution of the Electric Double-Layer to the Curvature Elasticity of Charged Amphiphilic Monolayers. *Physica A* **1989,** 159 (3), 319-328 DOI: 10.1016/0378-4371(89)90400-7.
35. Winterhalter, M.; Helfrich, W. Bending Elasticity of Electrically Charged Bilayers - Coupled Monolayers, Neutral Surfaces, and Balancing Stresses. *Journal of Physical Chemistry* **1992,** 96 (1), 327-330 DOI: 10.1021/j100180a060.
36. Loverde, S. M.; Solis, F. J.; de la Cruz, M. O. Charged Particles on Surfaces: Coexistence of Dilute Phases and Periodic Structures at Interfaces. *Physical Review Letters* **2007,** 98 (23), DOI: 10.1103/PhysRevLett.98.237802.
37. Seifert, U.; Berndl, K.; Lipowsky, R. Shape Transformations of Vesicles: Phase Diagram for Spontaneous- Curvature and Bilayer-Coupling Models. *Physical Review A* **1991,** 44 (2), 1182-1202 DOI: 10.1103/PhysRevA.44.1182.
38. Zhongcan, O. Y.; Helfrich, W. Instability and Deformation of a Spherical Vesicle by Pressure. *Physical Review Letters* **1987,** 59 (21), 2486-2488 DOI: 10.1103/PhysRevLett.59.2486.
39. Ortiz, V.; Nielsen, S. O.; Discher, D. E.; Klein, M. L.; Lipowsky, R.; Shillcock, J. Dissipative Particle Dynamics Simulations of Polymersomes. *Journal of Physical Chemistry B* **2005,** 109 (37), 17708-17714 DOI: 10.1021/jp0512762.
40. Li, X. J.; Pivkin, I. V.; Liang, H. J.; Karniadakis, G. E. Shape Transformations of Membrane Vesicles from Amphiphilic Triblock Copolymers: A Dissipative Particle Dynamics Simulation Study. *Macromolecules* **2009,** 42 (8), 3195-3200 DOI: 10.1021/ma9000918.
41. Chakraborty, K.; Vijayan, K.; Brown, A. E. X.; Discher, D. E.; Loverde, S. M. Glassy Worm-Like Micelles in Solvent and Shear Mediated Shape Transitions. *Soft Matter* **2018,** 14 (20), 4194-4203 DOI: 10.1039/C8SM00080H.
42. Shinoda, W.; DeVane, R.; Klein, M. L. Multi-Property Fitting and Parameterization of a Coarse Grained Model for Aqueous Surfactants. *Molecular Simulation* **2007,** 33 (1-2), 27-36 DOI: 10.1080/08927020601054050.
43. Drenscko, M.; Loverde, S. M. Characterisation of the Hydrophobic Collapse of Polystyrene in Water Using Free Energy Techniques. *Molecular Simulation* **2017,** 43 (3), 234-241.
44. Seo, S.; Shinoda, W. Spica Force Field for Lipid Membranes: Domain Formation Induced by Cholesterol. *Journal of Chemical Theory and Computation* **2019,** 15 (1), 762-774 DOI: 10.1021/acs.jctc.8b00987.

45. Percec, V.; Wilson, D. A.; Leowanawat, P.; Wilson, C. J.; Hughes, A. D.; Kaucher, M. S.; Hammer, D. A.; Levine, D. H.; Kim, A. J.; Bates, F. S.; Davis, K. P.; Lodge, T. P.; Klein, M. L.; DeVane, R. H.; Aqad, E.; Rosen, B. M.; Argintaru, A. O.; Sienkowska, M. J.; Rissanen, K.; Nummelin, S.; Ropponen, J. Self-Assembly of Janus Dendrimers into Uniform Dendrimersomes and Other Complex Architectures. *Science* **2010,** 328 (5981), 1009-1014 DOI: 10.1126/science.1185547.
46. Shinoda, W.; DeVane, R.; Klein, M. L. Coarse-Grained Force Field for Ionic Surfactants. *Soft Matter* **2011,** 7 (13), 6178-6186 DOI: 10.1039/C1SM05173C.
47. Chakraborty, K.; Shinoda, W.; Loverde, S. M. Molecular Simulation of the Shape Deformation of a Polymersome. *Soft Matter* **2020,** 16 (13), 3234-3244 DOI: 10.1039/c9sm02165e.
48. Shinoda, W.; DeVane, R.; Klein, M. L. Coarse-Grained Molecular Modeling of Non-Ionic Surfactant Self-Assembly. *Soft Matter* **2008,** 4 (12), 2454-2462.
49. Plimpton, S. Fast Parallel Algorithms for Short-Range Molecular Dynamics. *Journal of Computational Physics* **1995,** 117 (1), 1-19 DOI: http://dx.doi.org/10.1006/jcph.1995.1039.
50. Feller, S. E.; Zhang, Y.; Pastor, R. W.; Brooks, B. R. Constant Pressure Molecular Dynamics Simulation: The Langevin Piston Method. *The Journal of Chemical Physics* **1995,** 103 (11), 4613-4621 DOI: 10.1063/1.470648.
51. Parrinello, M.; Rahman, A. Polymorphic Transitions in Single-Crystals - a New Molecular-Dynamics Method. *Journal of Applied Physics* **1981,** 52 (12), 7182-7190 DOI: 10.1063/1.328693.
52. Martyna, G. J.; Tobias, D. J.; Klein, M. L. Constant-Pressure Molecular-Dynamics Algorithms. *Journal of Chemical Physics* **1994,** 101 (5), 4177-4189 DOI: 10.1063/1.467468.
53. Kästner, J. Umbrella Sampling. *Wiley Interdisciplinary Reviews: Computational Molecular Science* **2011,** 1 (6), 932-942 DOI: 10.1002/wcms.66.
54. Fiorin, G.; Klein, M. L.; Henin, J. Using Collective Variables to Drive Molecular Dynamics Simulations. *Molecular Physics* **2013,** 111 (22-23), 3345-3362 DOI: 10.1080/00268976.2013.813594.
55. Zhu, F.; Hummer, G. Convergence and Error Estimation in Free Energy Calculations Using the Weighted Histogram Analysis Method. *Journal of Computational Chemistry* **2012,** 33 (4), 453-465 DOI: 10.1002/jcc.21989.
56. Kumar, S.; Rosenberg, J. M.; Bouzida, D.; Swendsen, R. H.; Kollman, P. A. The Weighted Histogram Analysis Method for Free-Energy Calculations on Biomolecules. I. The Method. *Journal of Computational Chemistry* **1992,** 13 (8), 1011-1021 DOI: 10.1002/jcc.540130812.
57. Goetz, R.; Gompper, G.; Lipowsky, R. Mobility and Elasticity of Self-Assembled Membranes. *Physical Review Letters* **1999,** 82 (1), 221-224 DOI: 10.1103/PhysRevLett.82.221.
58. den Otter, W. K.; Briels, W. J. The Bending Rigidity of an Amphiphilic Bilayer from Equilibrium and Nonequilibrium Molecular Dynamics. *Journal of Chemical Physics* **2003,** 118 (10), 4712-4720 DOI: 10.1063/1.1543941.
59. Watson, M. C.; Penev, E. S.; Welch, P. M.; Brown, F. L. H. Thermal Fluctuations in Shape, Thickness, and Molecular Orientation in Lipid Bilayers. *Journal of Chemical Physics* **2011,** 135 (24), DOI: 10.1063/1.3660673.
60. Kawamoto, S.; Nakamura, T.; Nielsen, S. O.; Shinoda, W. A Guiding Potential Method for Evaluating the Bending Rigidity of Tensionless Lipid Membranes from Molecular Simulation. *The Journal of Chemical Physics* **2013,** 139 (3), 034108 DOI: 10.1063/1.4811677.
61. Watson, M. C.; Brandt, E. G.; Welch, P. M.; Brown, F. L. H. Determining Biomembrane Bending Rigidities from Simulations of Modest Size. *Physical Review Letters* **2012,** 109 (2), 028102 DOI: 10.1103/PhysRevLett.109.028102.
62. Cheetham, A. G.; Zhang, P. C.; Lin, Y. A.; Lock, L. L.; Cui, H. G. Supramolecular Nanostructures Formed by Anticancer Drug Assembly. *Journal of the American Chemical Society* **2013,** 135 (8), 2907-2910 DOI: 10.1021/ja3115983.

63. Cui, G.; Swails, J. M.; Manas, E. S. Spam: A Simple Approach for Profiling Bound Water Molecules. *Journal of Chemical Theory and Computation* **2013,** 9 (12), 5539-5549 DOI: 10.1021/ct400711g.